ADVANCED MATERIALS

DOI: 10.1002/adma.200701246

Anomalous Optical Properties of InN Nanobelts: Evidence of Surface Band Bending and Photoelastic Effects**

By *Szu Ping Fu*, *Chia Ju Yu*, *Tzung Te Chen*, *Geng Ming Hsu*, *Miin Jang Chen*, *Li Chyong Chen*,* *Kuei Hsien Chen*, and *Yang Fang Chen**

In the past few years InN, the least understood Group III nitride compound, has attracted a great deal of interest because of its unique properties, making it suitable for applications in various electronic and optoelectronic devices.[1–8] In addition, InN is considered as a potential material for low-cost, low-power-consumption, high-sensitivity detection in gas, vapors, and liquids by virtue of its intrinsic surface charge accumulation.[9–12] Consequently, the preparation and study of InN nanomaterials are of particular importance in the aforementioned devices owing to the high surface-to-volume ratio as compared to the bulk, a property which may largely enhance the operation efficiency. One-dimensional (1D) nanostructures are excellent systems in which one can investigate the dependence of their unique fundamental properties on dimensionality and their potential applications.[13–17] Recently, it has been demonstrated that wurtzite nanobelts have the potential of converting biological mechanical energy, vibration energy, and biofluid hydraulic energy into electricity, raising the tantalizing prospect of the self-powering of wireless nanodevices and nanosystems for optoelectronics, biosensors, and resonators.[18] Therefore, InN nanobelts are promising candidates for incorporation into the above-mentioned devices. Despite all these potential advantages of InN nanobelts studies on this material remain scarce, most probably because of the difficulties associated with the growth of belt-like nanostructures. In this Communication, we have discovered several unique behaviors based on the study of photoluminescence (PL) and Raman scattering spectra of high-quality InN nanobelts fabricated by the metal-organic chemical vapor deposition (MOCVD) technique. The PL spectra of these InN nanobelts exhibit an extraordinarily large blue-shift with increasing excitation intensity, as compared with their thin-film counterparts. In addition, we found that the phonon frequencies of InN nanobelts decrease with increasing excitation intensity. Surface band bending, piezoelectricity, and photoelastic effects were employed to explain these anomalous behaviors. Besides, temperature-dependent PL spectra are also consistent with the prediction of our proposed model.

Structural and morphological information of the as-synthesized InN nanobelts was obtained from scanning electron microscopy (SEM) images. Apparently, high-density belt-like structures with length of several tens of nanometers cover the substrate, as shown in Figure 1. A high-magnification SEM image (inset to Fig. 1) revealed that the morphologies of the nanobelts are well-faceted with smooth surfaces. A detailed examination of the nanobelts along their length showed that they were uniform in both width and thickness, ranging from 40 to 250 nm and 10 to 35 nm, respectively.

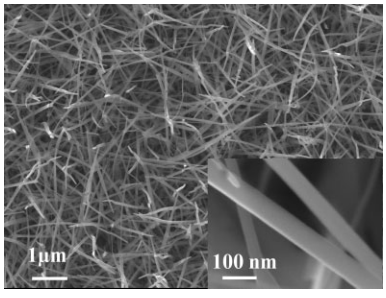

Figure 1. Low-magnification SEM image of InN nanobelts. Inset shows the high-magnification image of InN nanobelts with well-defined facets.

Typical PL spectra of the nanobelts measured at 20 K under different excitation intensities are shown in Figure 2a. A strong PL emission at 0.82 eV and blue-shifts of the PL spectra with increasing excitation intensity were observed. Figure 2b shows the evolution of the line width and integrated PL intensity with excitation intensity. The linear dependence of the integrated intensity, the broadening in the line width, and the blue-shift of the PL spectra with increasing excitation

[*] Dr. L. C. Chen, C. J. Yu, G. M. Hsu, Dr. K. H. Chen
Center for Condensed Matter Sciences
National Taiwan University
Taipei 10617 (Taiwan)
E-mail: chenlc@ccms.ntu.edu.tw
Prof. Y. F. Chen, Dr. S. P. Fu, T. T. Chen
Department of Physics
National Taiwan University
Taipei 10617 (Taiwan)
E-mail: yfchen@phys.ntu.edu.tw
C. J. Yu, Prof. M. J. Chen
Department of Materials Science and Engineering
National Taiwan University
Taipei 10617 (Taiwan)
Dr. K. H. Chen
Institute of Atomic and Molecular Sciences
Academia Sinica
Taipei 10617 (Taiwan)

[**] This work was supported by the National Science Council of the Republic of China.

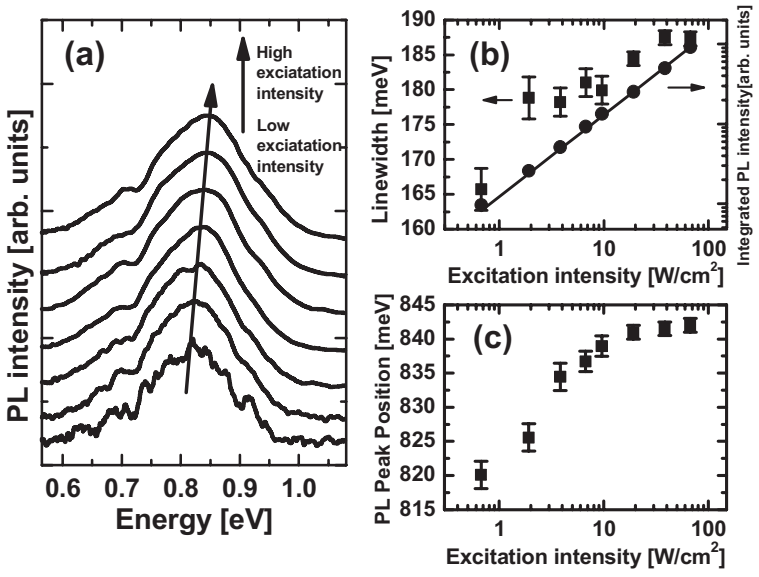

Figure 2. a) PL spectra of the InN nanobelts measured at 20 K under different excitation intensities. b) Evolutions of the line width and integrated PL intensity with excitation intensity. c) Evolution of the PL peak positions with excitation intensity.

intensity suggest that free-to-bound radiative recombination may be responsible for the PL emission throughout the near-IR region.[19-21] Figure 2c shows the evolution of the PL peak positions with excitation intensity, obtained from Figure 2a. We found that the PL peak position increased steadily with increasing excitation intensity within two orders of magnitude, and the magnitude of the blue-shift can be as large as 20 meV. For InN epifilms with similar PL peak position, the blue-shift of PL spectra is as little as ~1 meV.[22] Obviously, the blue-shifts of the PL spectra of nanobelts are anomalously large, indicating that other dominant mechanisms are responsible for the observed PL emission.

In order to understand the above behavior, we considered the unique inherent properties of nanobelts. One of the obvious features is the large surface-to-volume ratio. The influence of surface effects may be negligible in bulk crystals, but become very significant for the nanomaterial. It has been reported that surface band bending resulting from the intrinsic surface charge accumulation in InN material does exist.[9,10] This surface effect was revealed by measurements of the relations between the sheet carrier density and the layer thickness of InN thin films and capacitance-voltage profiling.[9] X-ray photoemission spectroscopy and high-resolution electron-energy loss spectroscopy measurements were then employed to further confirm this unique phenomenon among all the Group III nitrides.[10,23] The origin of the electron accumulation in InN is explained in terms of its band structure. It was shown that InN exhibited an unusually low conduction band minimum at the G point by means of ab initio calculations.[24] Thus, the Fermi stabilization energy, defined as the average midgap energy throughout the entire Brillouin zone (BZ), lies in the conduction band, resulting in the existence of the donor-like defects in the conduction band.[24] These states are capable of acquiring positive charge by emitting electrons into the conduction band. An electric field induced by these states pointing normally to the surface then exists in the surface region, leading to the electron accumulation and a downward band bending in this region.[9,10,23,24] According to the reported studies, the thickness of the accumulation layer is estimated to be several nanometers.[10,24] Let us now utilize this well-established surface band bending to explain our observed giant blue-shift. The observed PL emission now should include the recombination of the extreme high-density surface electrons and the photoholes distributed in the inner regions of the InN materials. This effect can be more pronounced in the nanobelts owing to the large surface-to-volume ratio. It is worth noting that the anomalously large CL and PL shifts have also been observed in ZnO and InN nanorods, wherein the shift, while detectable even far beyond the quantum-confinement regime, was found to be strongly size-dependent, indicating that surface effects might a play key role for the shift.[25,26] The schematic band diagrams showing the recombination mechanisms of the observed PL emission in InN nanobelts are given in Figure 3b and c. As the excitation intensity increases, the surface electric field induced by the donor-like defects is partially screened by the photon generated carriers, leading to an upward shift of

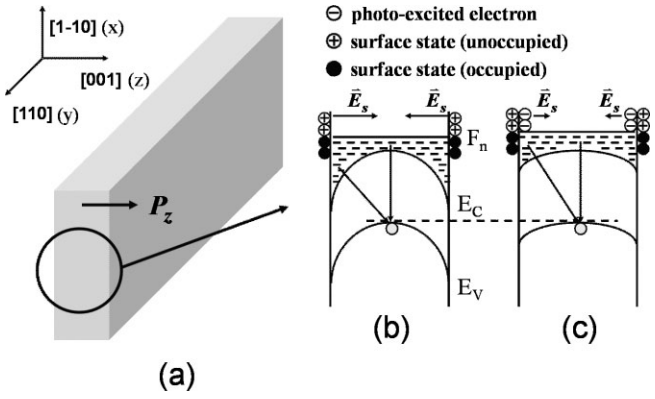

Figure 3. Schematic diagram of a) the crystallographic direction nanobelt, b) the band energy and surface electric field under low excitation intensity, and c) the band energy and surface electric field under high excitation intensity (E_C and E_V are the conduction and valence band, band edges, respectively, and F_n is the Fermi level in the conduction band).

both bands, which results in an "extra" blueshift of PL emission as shown in Figure 3c. Thus, the giant blue shift of PL spectra with increasing excitation intensity can be well understood.

In addition to influencing the PL spectra, the intrinsic surface band bending may also introduce a novel phenomenon known as the photoelastic effect. The photoelastic effect is de-

ADVANCED MATERIALS

fined as a change in the internal strain of a material induced by incident electromagnetic waves.[27] It is well known that Group III nitrides are piezoelectric materials with large piezoelectric constants compared to the other conventional Group III–IV and II–VI compounds.[28,29] Since the surface electric field has been well-established, the existence of the internal stress therefore can be expected based on the converse piezoelectric effect. Because the surface electric field will be partially screened after light excitation, it results in the apparent change of the internal stress, and the photoelastic effect should be observable in InN nanobelts owing to their large surface-to-volume ratio.

To justify our foregoing inference, the excitation-power-dependent Raman scattering measurements for InN nanobelts were then performed, as shown in Figure 4a. For the wurtzite crystal structure, group theory predicts at the Γ point the symmetry species $A_1 + E_1 + 2B_1 + 2E_2$. The polar phonon modes

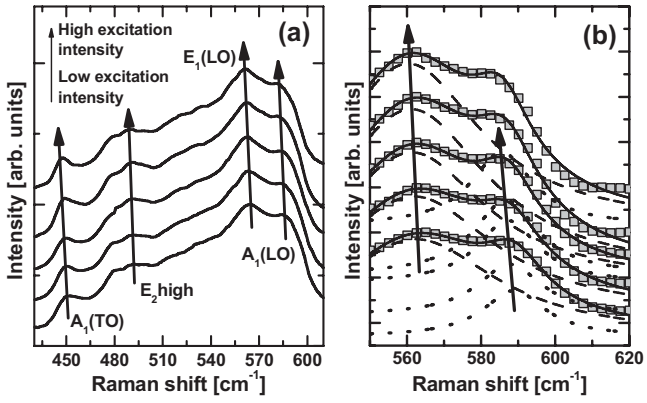

Figure 4. a) Excitation-intensity-dependent Raman scattering spectra of the InN nanobelts. The arrows indicate the red-shifts of A_1(TO), E_2 high, E_1(LO), and A_1(LO), from left to right, respectively. b) Lorentzian fits (solid line) for the E_1(LO) and A_1(LO) phonon modes. The dashed and dotted lines denote the derived E_1(LO) and A_1(LO) phonon modes.

of the A_1 and E_1 symmetry are Raman- and infrared-active and split into longitudinal (LO) and transverse (TO) components, while the nonpolar E_2 mode is Raman-active only.[30] The B_1 modes are both Raman- and infrared-inactive (silent). Thus, the peaks observed at ~560 cm^{-1}, 490 cm^{-1}, and 450 cm^{-1} are assigned to the E_1(LO), E_2 high, and A_1(TO) phonon modes of InN, respectively, whereas the high-energy shoulder observed at ~585 cm^{-1} is assigned to A_1(LO) mode. A careful line shape fitting of our Raman scattering spectra using the Lorentzian function was then performed to determine the E_1(LO) and A_1(LO) phonon frequencies precisely, as shown in Figure 4b. We found that the line widths of both the E_1(LO) and A_1(LO) phonon modes decrease slightly with increasing excitation intensity as shown in Figure 5a. Raman shifts of all observed phonon modes as a function of excitation intensity are shown in Figure 5b and c. Obviously, all the phonon modes of InN nanobelts exhibit red-shifts in frequency with increasing excitation intensity. Based on the line widths shown in Figure 5a and the blue-shift of the PL peak energy

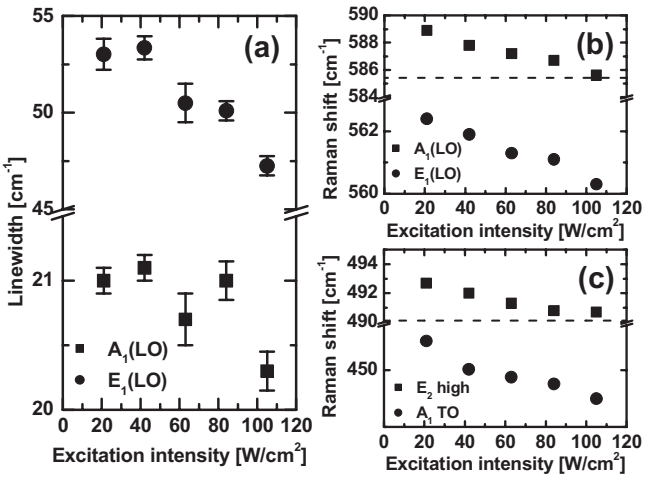

Figure 5. a) Raman linewidths of the A_1(LO) and E_1(LO) phonon modes as a function of excitation intensity. b) Raman frequencies of the A_1(LO) and E_1(LO) phonon modes as a function of excitation intensity. c) Raman frequencies of the E_2 high and A_1(TO) phonon modes as a function of excitation intensity.

with increasing excitation intensity, as shown in Figure 2a, we can rule out the possibility that the observed effect is due to a laser-induced self-heating effect.[31,32] The strain-free Raman frequencies for the E_2 high and A_1(LO) phonon modes are also shown in Figure 5b and c as the dash line, for comparison.[33] We can see that the frequencies of the E_2 high and A_1(LO) phonon modes of the InN thin film remain constant with increasing excitation intensity. This result is completely consistent with the prediction of the photoelastic effect, as outlined above. For the InN thin film, with its small surface-to-volume ratio, the influence of the built-in surface electric field is negligible, and therefore the photoelastic effect is hardly seen. However, for the InN nanobelts the surface effect becomes significant because of their large surface-to-volume ratio. Therefore, when the built-in surface electric field is screened by the photo-excited electron-hole pairs, the internal strain is also reduced and results in the observed red-shift in Raman phonon modes.

Let us now try to estimate the variation of internal strain versus excitation intensity. We first considered the piezoelectric polarization and uniaxial internal stress along the [001] direction, because this plane is the dominant one with a much larger area compared to the other planes, in the first order approximation. The piezoelectric polarization along [001] direction, P_Z, is simply expressed via the piezoelectric coefficients e_{33} and e_{13} as[29]

$$P_Z = e_{33}\varepsilon_3 + e_{31}(\varepsilon_1 + \varepsilon_2) \quad (1)$$

where ε_3 is the strain along the c axis, and ε_1 and ε_2 are the in-plane strains which we assumed to be isotropic. In the case of the uniaxial stress along the [001] direction, the relation of the in-plane and uniaxial strains can be described as[34]

$$\varepsilon_1 = -\frac{C_{13}}{C_{11} + C_{12}}\varepsilon_3. \quad (2)$$

where the C_{ij} elements are the stiffness constants for InN.[35] Thus, the piezoelectric polarization of the InN nanobelts along the [001] direction was then estimated to be $P_z = 1.24\ \varepsilon_3$, which may be counterbalanced by the noticeable surface electric field established by the surface donor-like defects, indicating that a compressive uniaxial strain along the [001] direction exists in the near-surface region, as shown in Figure 3a. The strength of the internal strain in the InN nanobelts can then be estimated according to the strain-induced phonon shifts, $\Delta\omega_i$, for quantitative explanation via the following expression[34]

$$\Delta\omega_i = 2a_1\varepsilon_1 + b_1\varepsilon_3 = \left(b_i - a_i\frac{2C_{13}}{C_{11}+C_{12}}\right)\varepsilon_3 \qquad (3)$$

where a_i and b_i are the deformation potential parameters of the respective phonon modes.[36] The calculations of the internal uniaxial strain along the [001] direction as a function of excitation intensity by means of the E_2 high phonon mode using Equation 3 are shown in Figure 6 as the solid squares. Apparently, the compressive strain, ε_3, exhibits a steady

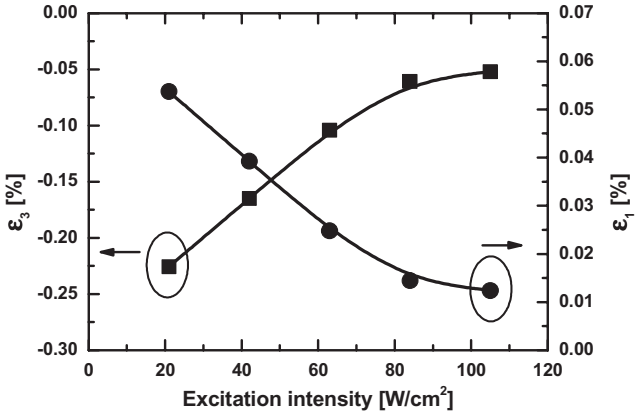

Figure 6. Calculated uniaxial strain ε_3 (solid squares) and in-plane strain ε_1 (solid circles) as a function of excitation intensity by the E_2 high (circles) phonon modes. The solid lines serve as guides for the eyes.

reduction from –0.22 % to –0.05 % with increasing excitation intensity which is consistent with the aforementioned discussions related to the photoelastic effect. In addition, the internal in-plane strains, ε_1 and ε_2, calculated by the combination of Equations 2 and 3 are also shown in Figure 6, for comparison. Obviously, the tensile in-plane strains ε_1 and ε_2 also show a steady reduction, from 0.06 % to 0.01 % with increasing excitation intensity. To further explore our inferences, high-resolution X-ray diffraction (XRD) experiments were performed, and the diffraction spectra of InN nanobelts and epifilm are shown in Figure 7 as dashed and solid lines, respectively. Clearly, we found that the (100) and (002) peaks showed a shift toward lower and higher diffraction angles, respectively, which suggests the existence of a compressive uniaxial strain along z axis and a tensile strain on x-y plane.

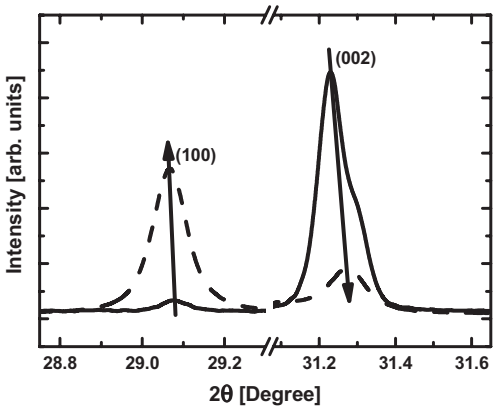

Figure 7. XRD spectra taken from InN nanobelts (dashed line) and thin film (solid line). The (100) and (002) peaks have been marked. The arrows indicate the downward or upward shifts of the respective peaks.

The estimated values of the respective strain calculated on the basis of the angle shifts are $\varepsilon_1 = 0.06$ % and $\varepsilon_3 = -0.2$ %, respectively, which is in excellent agreement with the values deduced by Raman shifts at low excitation intensity, providing another piece of evidence to support our proposed interpretation. The reduction of the tensile in-plane strain thus gives rise to a noticeable increase of the band-gap energy resulting in a considerable blue-shift of PL peak energy.[37,38] With GaN, for example, the change in band-gap energy has been found to be about 20 meV under an in-plane strain $\varepsilon_1 \sim 0.2\%$. For InN, the theoretical value has not been reported, but the estimated value is around several to several tens meV, which is in good agreement with our PL spectra.

Figure 8a and b shows the results of the temperature-dependent PL measurements under high and low optical excitation in order to further support our discussions based on the

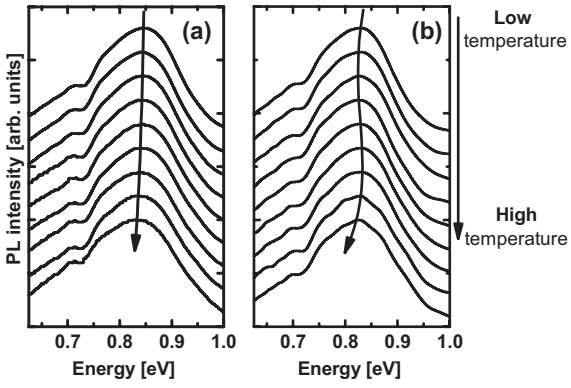

Figure 8. Temperature-dependent PL spectra under a) high excitation intensity, and b) low excitation intensity. The arrows denote the evolutions of the PL peak position with temperature.

photoelastic effect. Obviously, the obtained PL spectra reveal quite different characteristics with temperature under both optical excitation conditions. The temperature behavior of the PL energy under high excitation is similar to the bulk materi-

ADVANCED MATERIALS

al, while the temperature behavior of PL under low excitation shows an anomalous blue-shift in energy between 70–110 K, as shown in Figure 9. In accordance with the above mentioned discussions, the blue-shift of PL emission under low excitation can be expressed as the thermally induced screening of the intrinsic surface electric field. The frozen carriers at low temperature will become thermally activated with rising temperature; therefore, the partially screened surface electric field under low excitation can be further screened by these thermally activated carriers, leading to a blue-shift of PL spectra. Consequently, the observed temperature characters of PL reflect a competition between the blue-shifts caused by thermally induced screening of the surface electric field and the red-shifts arising from the thermal expansion and electron-phonon interaction. The thermal expansion and electron-phonon interaction play the dominant roles in mechanisms responsible for PL emission as the temperature exceeds 110 K, resulting in a gradual red-shift. In contrast with the PL characteristics under low excitation, the surface electric field is already screened out by optically generated carriers, leading to the monotonic red-shift of the PL peak energy resembling that of the bulk material. The result hence gives yet another strong piece of evidence to support the concept of the correlation between the PL emission, converse piezoelectric effect, and photoelastic effect.

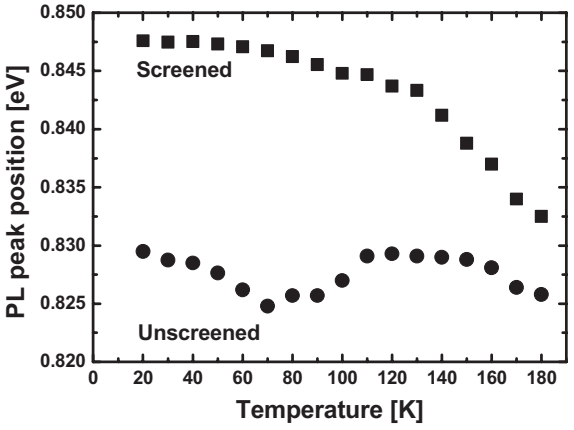

Figure 9. PL peak energy as a function of temperature under high (squares) and low (circles) excitation intensity.

In conclusion, this Communication presents several intriguing behaviors observed in MOCVD-grown, freestanding InN nanobelts synthesized on SiN_x-coated Si substrates. The PL spectra exhibit an anomalously large blue-shift with increasing excitation intensity as compared with InN thin films. In addition, we found that the phonon frequencies of the InN nanobelts decrease with increasing excitation intensity by Raman scattering measurements. Surface band bending, converse piezoelectric effect, and photoelastic effects are employed to explain the anomalously large shifts in detail. Temperature-dependent PL spectra under high and low optical excitation also provide a strong piece of evidence to support our interpretation. The research demonstrated in this Communication could pave a key path to manipulating the physical properties of InN nanobelts by external optical excitation, a necessary condition for the widespread applications of InN nanobelts in such diverse fields as optoelectronics, biosensors, and resonators. In addition, it is readily extended to the study of many other nanomaterials, because its underlying origin arises from the inherent large surface-to-volume ratio of the geometric structure.

Experimental

The InN nanobelts with the wurtzite structure used in this study were synthesized in a home-made MOCVD system on SiN-coated Si substrate using trimethylindium (TMIn) and NH_3 as precursors. During growth N_2 was used as the carrier gas. A thin layer of Au film (2 nm) was deposited on SiN_x-coated Si substrates by the dc sputtering technique, serving as the catalytic layer. Transmission electron microscopy (TEM) studies revealed that all the nanobelts grew along the [110] direction, and were enclosed only by $\pm(001)$ and $\pm(1\bar{1}0)$ facets. The synthesis of InN nanobelts was all performed at a temperature of 540 °C and a pressure of 1 Torr (1 Torr = 1.333×10^2 Pa) for 4 h. The PL measurements were conducted by using a semiconductor diode laser operating at 808 nm as the excitation source and an Electro-Optical Systems extended InGaAs detector. The excitation intensity was varied from 0.67 to 67 W cm^{-2}. Raman scattering measurements were performed in the backscattering geometry by a Jobin Yvon T64000 system working in triple-subtractive mode. An Ar^+ laser (γ = 488 nm) was used as a source of excitation and a neutral density filter was used as intensity controller.

Received: May 23, 2007

[1] A. G. Bhuiyan, A. Hashimoto, A. Yamamoto, *J. Appl. Phys.* **2003**, *94*, 2779.
[2] E. Bellotti, B. K. Doshi, K. F. Brennan, J. D. Albrecht, P. P. Ruden, *J. Appl. Phys.* **1999**, *85*, 916.
[3] S. K. O'Leary, B. E. Foutz, M. S. Shur, L. F. Eastman, *Appl. Phys. Lett.* **2005**, *87*, 222103.
[4] S. K. O'Leary, B. E. Foutz, M. S. Shur, L. F. Eastman, *Appl. Phys. Lett.* **2006**, *88*, 152113.
[5] V. Yu. Davydov, A. A. Klochikhin, R. P. Seisyan, V. V. Emtsev, S. V. Ivanov, F. Bechstedt, J. Furthmüller, H. Harima, A. V. Mudryi, J. Aderhold, O. Semchinova, J. Graul, *Phys. Status Solidi B* **2002**, *229*, R1.
[6] J. Wu, W. Walukiewicz, K. M. Yu, J. W. Ager, E. E. Haller, H. Lu, W. J. Schaff, Y. Saito, Y. Nanishi, *Appl. Phys. Lett.* **2002**, *80*, 3967.
[7] S. P. Fu, T. T. Chen, Y. F. Chen, *Semicond. Sci. Technol.* **2006**, *21*, 244.
[8] T. Matsuoka, H. Okamoto, M. Nakao, H. Harima, E. Kurimoto, *Appl. Phys. Lett.* **2002**, *81*, 1246.
[9] H. Lu, W. J. Schaff, L. F. Eastman, C. E. Stutz, *Appl. Phys. Lett.* **2003**, *82*, 1736.
[10] I. Mahboob, T. D. Veal, C. F. McConville, H. Lu, W. J. Schaff, *Phys. Rev. Lett.* **2004**, *92*, 036804.
[11] H. Lu, W. J. Schaff, L. F. Eastman, *J. Appl. Phys.* **2004**, *96*, 3577.
[12] O. Kryliouk, H. J. Park, H. T. Wang, B. S. Kang, T. J. Anderson, F. Ren, S. J. Pearton, *J. Vac. Sci. Technol. B* **2005**, *23*, 1891.
[13] Z. L. Wang, *Adv. Mater.* **2000**, *12*, 1295.
[14] J. Hu, T. W. Odom, C. M. Lieber, *Acc. Chem. Res.* **1999**, *32*, 435.
[15] Y. Xia, P. Yang, Y. Sun, Y. Wu, B. Mayers, B. Gates, Y. Yin, F. Kim, H. Yan, *Adv. Mater.* **2003**, *15*, 353.
[16] J. C. Johnson, H. J. Choi, K. R. Knutsen, R. D. Schaller, P. Yang, R. J. Saykally, *Nat. Mater.* **2002**, *1*, 106.

[17] M. Huang, S. Mao, H. Feick, H. Yan, Y. Wu, H. Kind, E. Weber, R. Russo, P. Yang, *Science* **2001**, *292*, 1897.

[18] J. Song, J. Zhou, Z. L. Wang, *Nano Lett.* **2006**, *6*, 1656.

[19] B. Arnaudov, T. Paskova, P. P. Paskov, B. Magnusson, E. Valcheva, B. Monemar, H. Lu, W. J. Schaff, H. Amano, I. Akasaki, *Phys. Rev. B* **2004**, *69*, 115216.

[20] A. A. Klochikhin, V. Yu. Davydov, V. V. Emtsev, A. V. Sakharov, V. A. Kapitonov, B. A. Andreev, H. Lu, W. J. Schaff, *Phys. Rev. B* **2005**, *71*, 195207.

[21] S. P. Fu, Y. F. Chen, K. Tan, *Solid State Commun.* **2006**, *137*, 203.

[22] M. S. Hu, G. M. Hsu, Chen, K. S. Yu, C. J. Hsu, H. C. Chen, L. C. Huang, J. S. Hong, L. S. Chen, Y. F. *Appl. Phys. Lett.* **2007**, *90*, 123109.

[23] K. A. Rickert, A. B. Ellis, F. J. Himpsel, H. Lu, W. J. Schaff, J. M. Redwing, F. Dwikusuma, T. F. Kuech, *Appl. Phys. Lett.* **2003**, *82*, 3254.

[24] I. Mahboob, T. D. Veal, L. F. J. Piper, C. F. McConville, H. Lu, W. J. Schaff, J. Furthmüller, F. Bechstedt, *Phys. Rev. B* **2004**, *69*, 201307.

[25] C. W. Chen, K. H. Chen, C. H. Shen, A. Ganguly. L. C. Chen, J. J. Wu, H. I. Wen, W. F. Pong, *Appl. Phys. Lett.* **2006**, *88*, 241905.

[26] Z. H. Lan, W. M. Wang, C. L. Sun, S. C. Shi, C. W. Hsu, T. T. Chen, K. H. Chen, C. C. Chen, Y. F. Chen, L. C. Chen, *J. Crystal Growth* **2004**, *269*, 87.

[27] J. F. Nye, *Physical Properties of Crystals*, Oxford University Press, New York, **1972**.

[28] A. Zoroddu, F. Bernardini, P. Ruggerone, V. Fiorentini, *Phys. Rev. B* **2001**, *64*, 045208.

[29] F. Bernardini, V. Fiorentini, D. Vanderbilt, *Phys. Rev. B* **1997**, *56*, R10024.

[30] C. A. Arguello, D. L. Rousseau, S. P. S. Porto, *Phys. Rev.* **1969**, *181*, 1351.

[31] X. D. Pu, J. Chen, W. Z. Shen, H. Ogawa, Q. X. Guo, *J. Appl. Phys.* **2005**, *98*, 033527.

[32] J. W. Pomeroy, M. Kuball, H. Lu, W. J. Schaff, X. Wang, A. Yoshikawa, *Appl. Phys. Lett.* **2005**, *86*, 223501.

[33] X. Wang, S. Che, Y. Ishitani, A. Yoshikawa, *Appl. Phys. Lett.* **2006**, *89*, 171907.

[34] J. M. Wagner, F. Bechstedt, *Appl. Phys. Lett.* **2000**, *77*, 346.

[35] K. Kim, W. R. L. Lambrecht, B. Segall, *Phys. Rev. B* **1996**, *53*, 16310.

[36] V. Darakchieva, P. P. Paskov, E. Valcheva, T. Paskov, P. Monemar, M. Schubert, H. Lu, W. J. Schaff, *Appl. Phys. Lett.* **2004**, *84*, 3636.

[37] V. Y. Davydov, N. S. Averkiev, I. N. Goncharuk, D. K. Nelson, I. P. Nikitina, A. S. Polkovnikov, A. N. Smirnov, M. A. Jacobson, O. K. Semchinova, *J. Appl. Phys.* **1997**, *82*, 5097.

[38] W. Shan, R. J. Hauenstein, A. J. Fischer, J. J. Song, W. G. Perry, M. D. Bremser, R. F. Davis, B. Goldenberg, *Phys. Rev. B* **1996**, *54*, 13460.

